

A Computational Reaction–Diffusion Model for the Analysis of Transport-Limited Kinetics

Ravi A. Vijayendran,[†] Frances S. Ligler,[‡] and Deborah E. Leckband^{†,§,*}

Department of Chemical Engineering and Center for Biophysics and Computational Biology, University of Illinois at Urbana–Champaign, Urbana, Illinois 61801, and Center for Bio/Molecular Science and Engineering, Naval Research Laboratory, Code 6900, Washington, D.C. 20375

Optical, evanescent wave biosensors have become popular tools for quantitatively characterizing the kinetic properties of biomolecular interactions. Analyzing data from biosensor experiments, however, is often complicated when mass-transfer influences the detection kinetics. We present a computational, transport–kinetic model that can be used to analyze transport-limited biosensor data. This model describes a typical biosensor experiment in which a soluble analyte diffuses through a flow chamber and binds to a receptor immobilized on the transducer surface. Analyte transport in the flow chamber is described by the diffusion equation while the kinetics of analyte–surface association and dissociation are captured by a reactive boundary condition at the sensor surface. Numerical integration of the model equations and non-linear least-squares fitting are used to compare model kinetic data to experimental results and generate estimates for the rate constants that describe analyte detection. To demonstrate the feasibility of this model, we use it to analyze data collected for the binding of fluorescently labeled trinitrobenzene to immobilized monoclonal anti-TNT antibodies. A successful analysis of this antigen–antibody interaction is presented for data collected with a fluorescence-based fiber-optic immunoassay. The results of this analysis are compared with the results obtained with existing methods for analyzing diffusion-limited kinetic data.

Optical, evanescent wave biosensors have become useful tools for characterizing the thermodynamic and kinetic properties of biomolecular interactions. Receptor–ligand, antigen–antibody, signal transduction, protein–DNA, and many other interactions have been studied with optical biosensors.¹ In these devices, unlike in solution, one of the molecules in the interaction of interest is immobilized on the sensor surface. The binding interaction is then observed when a second reactant, the analyte, is introduced into the solution bathing the immobilized binding partner. Complex formation is monitored by recording changes in the index of refraction or fluorescence emission at the sensor surface.

[†] Department of Chemical Engineering, University of Illinois at Urbana–Champaign.

[‡] Naval Research Laboratory.

[§] Center for Biophysics and Computational Biology, University of Illinois at Urbana–Champaign.

(1) Schuck, P. *Ann. Rev. Biophys. Biomol. Struct.* **1997**, *26*, 541–566.

To obtain kinetic information from these experiments, it is necessary to have a mathematical model of the binding/unbinding dynamics. A simple model can be constructed by analytically solving the kinetic rate equation that describes analyte–surface binding. Assuming a simple bimolecular, first-order interaction with an association rate constant k_f and a dissociation rate constant k_r , the rate equation governing the time evolution of analyte binding is given by the following expression.

$$dc_b(t)/dt = k_f c(c_{b,\text{sat}} - c_b) - k_r c_b \quad (1)$$

If no analyte is bound at the beginning of the experiment, the solution to the above equation is given by

$$c_b(t) = \frac{k_f c_{b,\text{sat}} c(1 - e^{-(k_f c + k_r)t})}{k_f c + k_r} \quad (2)$$

In the preceding expressions, c is the analyte concentration in the bulk solution, c_b is the density of bound complex on the surface, and $c_{b,\text{sat}}$ is the density of binding sites on the surface, representing the maximum possible value of c_b . Equations 1 and 2 do not describe analyte transport to the fiber surface. This model, therefore, assumes that the detection kinetics are reaction-rate-limited and that the analyte concentration is constant and uniform everywhere above the sensor surface. Because of these limitations, we refer to the above equations as the “well-mixed” model. In a typical experiment, the model’s assumptions can be satisfied by continuously flowing analyte over the sensor surface.

When the detection kinetics are limited by mass transfer, a number of studies have applied a two-compartment model.^{2,3} Like the well-mixed model, this approach assumes a spatially homogeneous supply of analyte at a concentration c_f , which is assumed to be constant throughout the experiment. Unlike the previous model, however, this distribution of analyte is confined to a compartment in the bulk solution far away from the sensor surface. A spatially uniform distribution of analyte at concentration $c(t)$ is also assumed to exist in an inner compartment of height h_i near the sensor surface. The analyte concentration in this compartment can change over time. The movement of analyte

(2) Myszka, D. G.; Morton, T. A.; Doyle, M. L.; Chaiken, I. M. *Biophys. Chem.* **1997**, *64*, 127–137.

(3) Myszka, D. G.; He, X.; Dembo, M.; Morton, T. A.; Goldstein, B. *Biophys. J.* **1998**, *75*, 583–594.

between the two compartments is described by a phenomenological rate constant k_m that accounts for both the convective and diffusive transport of analyte across the intervening layer between the bulk solution and the sensor surface. Mathematically, this situation is described by the following ordinary differential equations.

$$\frac{dc(t)}{dt} = \frac{1}{h_i} [-k_f c(c_{b,\text{sat}} - c_b) + k_r c_b + k_m(c_T - c)] \quad (3)$$

$$\frac{dc_b(t)}{dt} = k_f c(c_{b,\text{sat}} - c_b) - k_r c_b \quad (4)$$

Typically, $c(t)$ is assumed to have reached a quasi steady state so that $dc/dt = 0$. Equations 3 and 4 are then combined so that the time evolution of analyte binding is given by the following expression, which is independent of h_i .

$$\frac{dc_b(t)}{dt} = \left[1 + \frac{k_f(c_{b,\text{sat}} - c_b)}{k_m} \right]^{-1} [k_f c_T(c_{b,\text{sat}} - c_b) - k_r c_b] \quad (5)$$

The preceding equation can be solved numerically and fit to kinetic data. With this approach, other researchers have been able to use the two-compartment model to estimate kinetic rate constants from biosensor data.^{2,3}

The two-compartment model is based on a simplistic view of the reaction–diffusion process. To accommodate such a simple description, the concentration of analyte within each compartment must be spatially homogeneous. As with the well-mixed model, experiments analyzed with the two-compartment model are typically done with a flowing analyte in order to satisfy this assumption. Despite this, for binding under highly transport-limited conditions, it has been found that the distribution of bulk analyte can exhibit spatial heterogeneity and moving-front phenomena that can cause the two-compartment model to break down.⁴ Therefore, although it has been applied successfully in previous studies, the two-compartment approach may not be able to describe diffusion-limited data in all cases.

In the two models presented thus far, assumptions regarding the distribution of analyte above the sensor surface restrict each model's applicability. In this work, we employ an alternative, computational, transport–kinetic model for analyzing biosensor data that is free of such limitations. Our model realistically describes the transport of analyte to the sensor surface with the diffusion equation. A reactive boundary condition containing the expression seen in previous models and the rate equation that describes the kinetics of analyte detection are used to build the details of analyte–surface binding into our analysis. The model is thus governed by the following,

$$\frac{\partial c}{\partial t} = D\nabla^2 c \quad \text{in the analyte solution} \quad (6)$$

$$D \frac{\partial c}{\partial n} = k_f c(c_{b,\text{sat}} - c_b) - k_r c_b \quad \text{at the sensor surface} \quad (7)$$

$$\frac{dc_b}{dt} = k_f c(c_{b,\text{sat}} - c_b) - k_r c_b \quad \text{at the sensor surface} \quad (8)$$

where D is the analyte diffusivity, n is the spatial coordinate normal

to the sensor surface, and ∇ is the gradient operator. After imposing initial and additional boundary conditions, the above equations are solved numerically to generate theoretical values of the bound concentration of analyte c_b as a function of time. These model data are fit to actual experimental results with a nonlinear least-squares algorithm to obtain estimates for the rate constants, binding site density, and analyte diffusivity.

Our transport-kinetic model provides a more rigorous description of a biosensor experiment than the two-compartment and well-mixed models. By solving eqs 6–8, one can track changes both in the analyte bound to the surface and free in solution over the course of an experiment. Therefore, no assumptions about the spatial distribution of analyte above the sensor surface need to be made. Highly transport-limited experiments that are characterized by an inhomogeneous distribution of analyte above the sensor surface can be accurately described. At the same time, experiments in which transport limitations are absent and the analyte solution is well-mixed are also described by our model as a special limiting case. The more exact description thus allows our model to accommodate a wider range of experimental conditions.

However, while the two-compartment and well-mixed models are used to analyze experiments done with flowing analyte, our model is restricted to describing experiments performed in the absence of flow under static conditions. Although eq 6 describes analyte diffusion, it does not account for the convection of analyte above the sensor surface. In its current form, our model cannot describe how changes in flow rate might impact the binding dynamics. It is possible to add a convection term to eq 6 and extend the model to also describe flow effects, but we leave this for a future study. Instead, in this work, we focus on demonstrating that the model provides a reasonable description both of analyte diffusion and of the detection kinetics.

To test our model, we used it to analyze the binding of trinitrobenzene (TNB) to a monoclonal 11B3 anti-TNT antibody. Several experiments were first performed under flowing conditions to evaluate the importance of transport effects in this antibody–antigen system. Due to TNB's small size, we did not observe any diffusion limitations for binding in aqueous buffers. However, by repeating the same experiments with glycerol, we were able to decrease the analyte's diffusivity and introduce transport limitations into the binding dynamics. In this work, the data from these experiments are analyzed with the two-compartment and well-mixed models. The results of these analyses are then compared with those of our model. As mentioned, eqs 5 and 6 cannot be applied when analyte is flowing over the sensor surface. To evaluate our model, therefore, the above experiments are repeated in the absence of flow. We successfully apply our model to these experiments and show that it can provide reasonable estimates for the rate constants both in the presence and in the absence of observable transport effects.

MATERIALS AND METHODS

Transport–Kinetic Model. The general geometrical model of the fiber-optic biosensor is illustrated in Figure 1. Due to the biosensor's axisymmetric geometry, it is sufficient to consider analyte transport within a plane that contains the center line of the fiber. Within this plane, the fiber is represented by a wall that extends for a length L and is tapered from radius h_1 to radius h_2 . The radius of the fiber at any position along its length

(4) Schuck, P. *Biophys. J.* **1996**, *70*, 1230–1249.

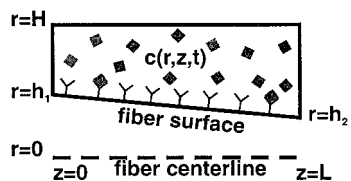


Figure 1. Geometrical model of the fiber-optic biosensor experiment. The figure is not drawn to scale. In reality, the length of the fiber is ~ 100 times larger than the inner diameter of the capillary wall.

is given by the following expression.

$$S(z) = h_1 + \frac{h_2 - h_1}{L} z \quad (9)$$

The analyte solution sits above the fiber and is bounded by the capillary wall at radius H . Within this volume, analyte transport is governed by eq 6 expressed in cylindrical coordinates.

$$\frac{\partial c}{\partial t} = \frac{D}{r} \left\{ \frac{\partial}{\partial r} \left(r \frac{\partial c}{\partial r} \right) + \frac{\partial^2 c}{\partial z^2} \right\} \quad (10)$$

Here, r and z are the spatial coordinates perpendicular and parallel to the fiber's center line, respectively. On the surface, the binding and unbinding of analyte is determined by eq 8. The capillary wall and the boundaries on either side of the analyte solution are assumed to be unreactive and impermeable. Therefore, the analyte flux normal to these boundaries is zero, and the following boundary conditions must be satisfied.

$$\frac{\partial c}{\partial r} = 0 \quad \text{at } r = H \quad (11a)$$

$$\frac{\partial c}{\partial z} = 0 \quad \text{at } z = 0 \quad \text{and } z = L \quad (11b)$$

The flux normal to the fiber surface is determined by the rate of the analyte–antibody binding reaction. We assume that the binding of Cy5-TNB to the 11B3 antibody is described by a first-order rate process so that eq 7 can be used as the boundary condition at the sensor surface. For the tapered geometry of the fiber, dc/dn is strictly a function of both dc/dr and dc/dz . Since $h_1 - h_2 \ll L$, however, eq 7 is approximately given by the following boundary condition.

$$D \frac{\partial c}{\partial r} = k_f c (c_{b,\text{sat}} - c_b) - k_r c_b \quad \text{at } r = S(z) \quad (11c)$$

To complete the model, initial conditions must also be specified. In our experiments, binding is initiated by rapidly injecting the sample above the fiber. Our model assumes that the injection rate is much faster than the rate of binding. If the analyte solution is assumed to be well-mixed by the injection, the initial distribution of analyte is then given by the following expressions.

$$c(r,z,t) = c_0 \quad \text{at } t = 0 \quad (12a)$$

$$c_b(z,t) = 0 \quad \text{at } t = 0 \quad (12b)$$

Model data are generated by solving the initial boundary value

problem given by the above equations. To do this, it is advantageous to recast these equations in terms of the following nondimensional quantities.

$$\begin{aligned} t &= \frac{Dt}{H^2} & \hat{r} &= \frac{r}{H} & \hat{c} &= \frac{c}{c_0} & \hat{z} &= \frac{z}{L} \\ & & & & \hat{c}_b &= \frac{c_b}{c_{b,\text{sat}}} & \hat{s} &= \frac{S(z)}{H} \end{aligned} \quad (13)$$

The model expressed in terms of these variables is given by the following.

$$\frac{\partial \hat{c}}{\partial \tau}(\hat{r}, \hat{z}, \tau) = \frac{1}{\hat{r}} \frac{\partial \hat{c}}{\partial \hat{r}} + \frac{\partial^2 \hat{c}}{\partial \hat{r}^2} + \frac{H^2}{L^2} \frac{\partial^2 \hat{c}}{\partial \hat{z}^2} \quad (14a)$$

$$\frac{d\hat{c}_b}{d\tau} = \frac{k_f \hat{c} c_0 H^2}{D} (1 - \hat{c}_b) - \frac{k_r \hat{c}_b H^2}{D} \quad \text{at } \hat{r} = \hat{s} \quad (14b)$$

$$\frac{\partial \hat{c}}{\partial \hat{r}}(\hat{r}, \hat{z}, \tau) = \frac{k_f \hat{c} H}{D} (1 - \hat{c}_b) - \frac{k_r \hat{c}_b c_{b,\text{sat}} H}{c_0 D} \quad \text{at } \hat{r} = \hat{s} \quad (14c)$$

$$\hat{c}(\hat{r}, \hat{z}, \tau) = 1 \quad \text{at } \tau = 0 \quad (14d)$$

$$\hat{c}_b(\hat{r}=0, \hat{z}, \tau) = 0 \quad \text{at } \tau = 0 \quad (14e)$$

$$\frac{\partial \hat{c}}{\partial \hat{z}}(\hat{r}, \hat{z}, \tau) = 0 \quad \text{at } \hat{z} = 0 \quad \text{and } \hat{z} = 1 \quad (14f)$$

$$\frac{\partial \hat{c}}{\partial \hat{r}}(\hat{r}, \hat{z}, \tau) = 0 \quad \text{at } \hat{r} = 1 \quad (14g)$$

Solving the above nondimensional model explicitly by the method of lines generated the model kinetic data.⁵ The time derivatives were integrated with a fifth order Runge–Kutta–Fehlberg algorithm while spatial derivatives were approximated with second-order finite difference formulas. Finite difference formulas were implemented in a modified coordinate system that mapped the tapered geometry of Figure 1 into a rectangular domain.⁶ A computational grid containing 11 and 21 equally spaced node points was imposed along the height and width of the modified coordinate system, respectively. Model kinetic data were fit to experimental data via a nonlinear least-squares algorithm. The four fitted constants, namely, the binding site density $c_{b,\text{sat}}$, the kinetic rate constants k_f and k_r , and analyte diffusivity D , were adjusted via the Levenberg–Marquardt method to minimize the difference between the model and experimental data.⁷ To ensure that the actual minimum had been reached, this fitting procedure was repeated several times with different initial guesses for the model parameters.

Two-Compartment Model. A similar approach was used to analyze kinetic data with the two-compartment model. After imposing the initial condition $c_b(t=0) = 0$, eq 7 was solved numerically with a Runge–Kutta–Fehlberg algorithm. The nu-

(5) Schiesser, W. E. *The Numerical Method of Lines Integration of Partial Differential Equations*; Academic Press Inc.: New York, 1991.

(6) Lindquist, C. K. M.S. Thesis, State University of New York at Buffalo, Buffalo, NY, 1998.

(7) Press: W. H.; Teukolsky, S. A.; Vetterling, W. T.; Flannery, B. P. *Numerical Recipes in C The Art of Scientific Computing*, 2nd ed.; Cambridge University Press: Cambridge, 1997.

merical solutions were then fit to experimental data via a Levenberg–Marquardt nonlinear least-squares routine. The kinetic rate constants, binding site density, and transport rate constant were adjusted until the difference between the model and experimental data was minimized.

Antibodies and Supplementary Reagents. The anti-TNT 11B3 monoclonal antibody and cyanine 5-ethylenediamine-labeled TNB (Cy5-TNB) were generated as previously described.⁸ The following reagents were also used: glycerol (Aldrich; Milwaukee, WI); bovine serum albumin (BSA), Tween-20 (T-20), goat IgG, and NaN_3 (Sigma; St. Louis, MO); ethanol (200 proof; Warner-Graham, Cockeysville, MD).

Fiber-Optic Biosensor and Fiber Preparation. All experiments were performed with the Analyte 2000 biosensor (Research International, Woodinville, WA) that has been described previously.⁹ The Analyte 2000 is equipped with a 635-nm diode laser that is capable of exciting Cy5 fluorescence. Excitation light from the laser is coupled to a fiber-optic probe. As light propagates along the length of the fiber via total internal reflection, fluorescent molecules near the fiber surface are excited. The emitted light, which has a longer wavelength than the excitation light, is coupled back through the fiber so that its intensity can be quantified by an attached fluorometer.

The preparation of the fiber-optic probes has been described extensively.¹⁰ Briefly, the fiber-optic probes were constructed from 600- μm -diameter, plastic-clad, silica fibers (Quartz Products, Tuckerton, DE). The sensing region of the fiber was formed by removing the plastic cladding that surrounds the last 12.5 cm of the probe. This region was then tapered with hydrofluoric acid to a diameter of 100 μm at the fiber's distal end.

The monoclonal 11B3 anti-TNT antibody was attached to the fiber surface following the procedure outlined by Bhatia et al.¹¹ The fibers were chemically modified with a 2% thiol-terminated silane ((3-mercaptopropyl)trimethoxysilane, Fluka, Hauppauge, NY) and then incubated in a 2 mM heterobifunctional cross-linker solution (*N*-succinimidyl-4-maleimidobutyrate, Fluka). The cross-linker's maleimide moiety reacts with the thiol group on the silane. This leaves the cross-linker's succinimide residue available to form stable, amide bonds with the antibody. After exposure to the cross-linker, the fibers were washed with water and then incubated in a 0.05 mg/mL solution of 11B3 anti-TNT antibody in phosphate-buffered saline (PBS), 0.01% NaN_3 , pH 7.4, for 1 h. Each antibody-coated fiber was then finally sealed within a flow chamber that was constructed from a 100- μL glass capillary tube capped by T-connectors at both ends.

Kinetic Assays. Two sets of experiments were performed under flowing conditions. In the first, binding was observed with 3, 5, 7, and 10 ng/mL Cy5-TNB diluted in a running buffer that contained PBS mixed with 2 mg/mL BSA and 0.1% T-20 (PBS/BSA/T-20). In the second set, binding was observed with the same analyte concentrations diluted in a running buffer that contained PBS/BSA/T-20 and 60 wt % glycerol. To observe binding, ~ 5 mL

of analyte solution was passed over the fiber surface with a syringe pump. Experiments were done at three different flow rates: 0.1, 0.5, and 1.0 mL/min. As the analyte bound, data were collected every 20 s. A different fiber was used for each experiment. However, within each experiment, data for all four concentrations were obtained with the same fiber. This was done by regenerating the fiber surface with a 1:1 mixture of ethanol and PBS between runs with successively increasing concentrations of Cy5-TNB. This regeneration step has been shown to have a negligible effect on the activity of the fiber's surface.¹² The binding at each concentration was observed twice to ensure reproducibility.

Following the above procedure, we also performed two additional sets of experiments in the absence of flow with the same concentrations of Cy5-TNB. One set was completed with analyte solutions prepared with PBS/BSA/T-20 while the other was done with solutions that contained 60 wt % glycerol and PBS/BSA/T-20 buffer. In these assays, instead of passing analyte solutions over the fiber, ~ 0.5 mL of analyte solution was injected over the fiber surface and allowed to bind without flow for 10 min. Again, different fibers were used for each experiment. However, within each experiment, a single fiber was used multiple times to observe the concentration dependence of the binding kinetics.

At the conclusion of each experiment, the fiber was saturated with a 200 ng/mL solution of Cy5-TNB for 10 min. In separate experiments, we have found that this procedure is sufficient to saturate the majority of the immobilized antibodies, and therefore, gives the intensity corresponding to $c_{b,\text{sat}}$. After the surface was saturated, the fiber was rinsed with running buffer and the intensity of the fluorescent signal was immediately recorded. All data recorded earlier in the experiment were normalized by this signal so that the kinetic data are expressed in terms of fractional coverage $c_b(t)/c_{b,\text{sat}}$. The antibody density $c_{b,\text{sat}}$ was not quantified directly for each fiber, but is one of the four fitted parameters. These fitted values were, however, within a factor of 2 of average antibody coverages determined by radiolabeling. The use of the normalized parameter, which was measured directly, allowed us to adjust the kinetic data for fiber-to-fiber optical variations.

Control Experiments. In addition to analyte that was bound to the immobilized antibodies, analyte that nonspecifically binds to the sensor surface and analyte that is in the bulk solution near the sensor surface can contribute to the fluorescence signal that one measures. These effects must be minimized in order to study the interaction between Cy5-TNB and the 11B3 antibody. We performed control experiments to quantify the importance of nonspecifically bound and bulk analyte in our measurements. In these experiments, the same fibers, which were used for the previously described kinetic assays, were cleaned by dipping them in HF for several minutes and then rinsing them with water. Using the above procedures, we then immobilized goat IgG and conducted kinetic assays with these fiber-optic probes. In all of the assays with goat IgG, the total signal was less than 10% of the total signal that was measured in the assays with the 11B3 anti-TNT antibody. Assuming that the nonspecific adsorption characteristics of Cy5-TNB are the same on goat IgG and the 11B3 antibody, this result shows that the contributions from nonspecific adsorption and bulk analyte are negligible compared to the signal

(8) Whelan, J. P.; Kusterbeck, A. W.; Wemhoff, G. A.; Bredehorst, R.; Ligler, F. S. *Anal. Chem.* **1993**, *65*, 3561–3565.

(9) Narang, U.; Anderson, G. P.; Ligler, F. S.; Burans, J. *Biosen. Bioelectron.* **1997**, *12*, 937–945.

(10) Golden, J. P.; Shriver-Lake, L. C.; Anderson, G. P.; Thompson, R. B.; Ligler, F. S. *Opt. Eng.* **1992**, *31*, 1458–1462.

(11) Bhatia, S. K.; Shriver-Lake, L. C.; Prior, K. J.; Georger, J.; Calvert, J. M.; Bredehorst, R.; Ligler, F. S. *Anal. Biochem.* **1989**, *178*, 408–413.

(12) Wijesuriya, D.; Breslin, K.; Anderson, G.; Shriverlake, L.; Ligler, F. S. *Biosen. Bioelectron.* **1994**, *9*, 585–592.

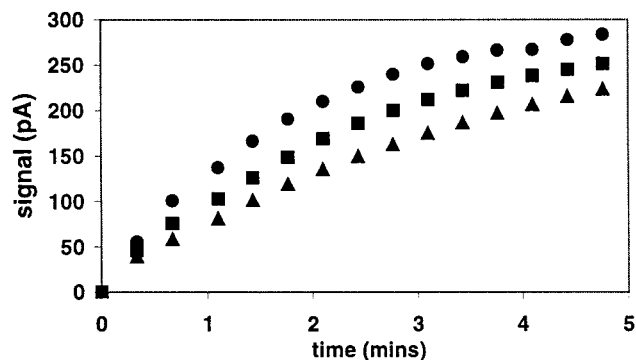


Figure 2. Increase of the rate of binding with the flow rate in the presence of glycerol. The raw signal from the biosensor's fluorometer is presented as a function of time for three different flow rates: 0.1 (triangles), 0.5 (squares), and 1 (circles) mL/min.

that arises from the specific binding of the Cy5-TNB to the anti-TNT antibody.

RESULTS

Before analyzing data with our computational model, it was necessary to confirm that the binding of Cy5-TNB to the 11B3 antibody was influenced by mass transport. One method to test for diffusion limitations is to increase the flow rate of analyte and look for concomitant changes in the binding rate.^{1,2} This was done for binding in both PBS and in PBS/glycerol solutions. In PBS, the binding rate was independent of the flow rate (data not shown). However, in the presence of glycerol, Figure 2 shows that increasing the analyte flow rate from 0.1 to 1.0 mL/min yielded substantially faster binding. Thus, while transport effects may not affect the reaction kinetics in PBS, they do play a role in the PBS/glycerol mixture.

Given the results in Figure 2, we decided to use a flow rate of 0.5 mL/min for the remainder of the experiments done under flowing conditions. This choice allowed us to use reasonable injection volumes (5 mL) and to also obtain transport-influenced binding. Figure 3 shows kinetic data from these experiments along with least-squares fits to the well-mixed model. For all of the experiments done under flowing conditions, the well-mixed model provided a qualitatively good description of the data. Table 1 lists the rate constants estimated with this model. The forward and reverse rate constants for experiments in PBS exceed the corresponding values for experiments done with PBS/glycerol mixtures. This may be a manifestation of the transport limitations that appear in these experiments. However, differences in the rate constants may also be due to changes in affinity that accompany sufficiently high concentrations of glycerol. A comparison of the equilibrium surface coverages in Figure 3 indicates that the affinity is lower for binding in the PBS/glycerol running buffer. Such changes in binding will impact the rate constants that one measures.

To evaluate the two-compartment model, we used it to analyze the data in Figure 3. The results of this analysis are presented in Figures 4. Like the well-mixed model, the two-compartment approach provided a reasonable description of the data. Table 2 shows that the two-compartment approach yielded rate constant estimates that were comparable to those produced by the well-mixed model. For the experiments in the PBS/glycerol mixture,

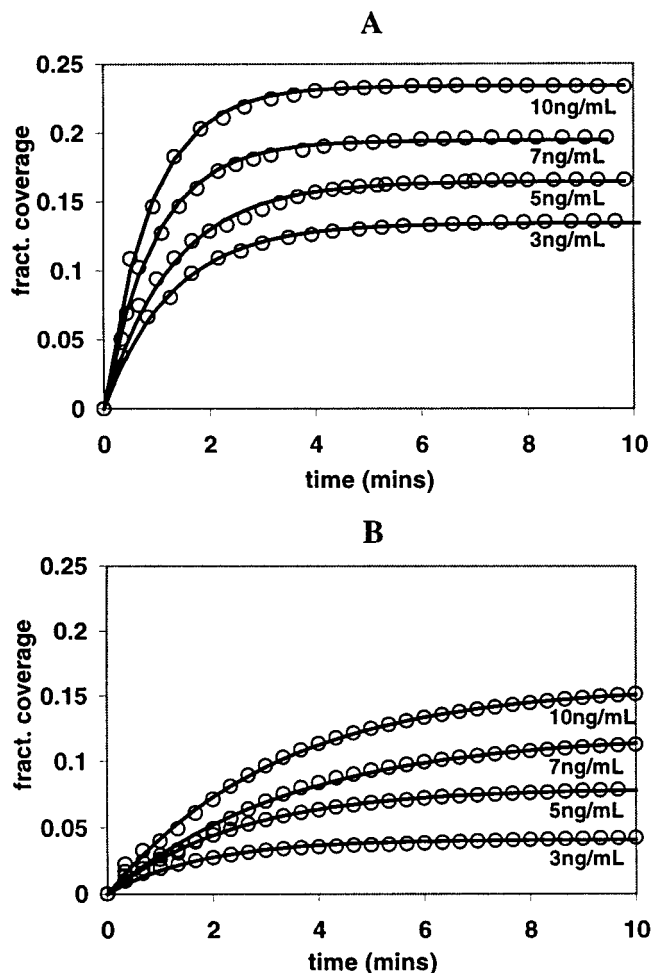


Figure 3. Analysis of kinetic data (circles) with the well-mixed model. Experiments were done under flowing conditions with analyte solutions containing PBS (A) and solutions containing PBS with 60 wt % glycerol (B). The solid lines show least-squares fits to the well-mixed model (eq 2).

Table 1. Parameters Estimated with the Well-Mixed Model for the Experiments Done under Flowing Conditions^a

concn, ng/mL	PBS		PBS + glycerol	
	$k_f, 10^5 \text{ M}^{-1} \text{ s}^{-1}$	$k_r, 10^{-2} \text{ s}^{-1}$	$k_f, 10^5 \text{ M}^{-1} \text{ s}^{-1}$	$k_r, 10^{-2} \text{ s}^{-1}$
3	5.6 ± 0.2	1.1 ± 0.04	1.3 ± 0.08	0.91 ± 0.04
5	3.9 ± 0.1	1.1 ± 0.04	0.99 ± 0.009	0.63 ± 0.04
7	4.5 ± 0.1	1.4 ± 0.06	0.77 ± 0.03	0.42 ± 0.06
10	4.4 ± 0.1	1.4 ± 0.06	0.78 ± 0.02	0.43 ± 0.04

^a Error estimates are calculated from the standard error for each parameter.

however, the two-compartment approach yielded on and off rates that were ~ 4 times larger. The two-compartment model accounts for the lower diffusivity and transport limitations that accompany the introduction of glycerol while the well-mixed model does not. For the experiments with glycerol, this suggests that transport effects rather than affinity changes lower the values of the rate constants estimated with the well-mixed model (Table 1). The two-compartment approach also yielded estimates for the binding site density and transport rate constant. The values for these parameters are reasonable. The good agreement between the estimates

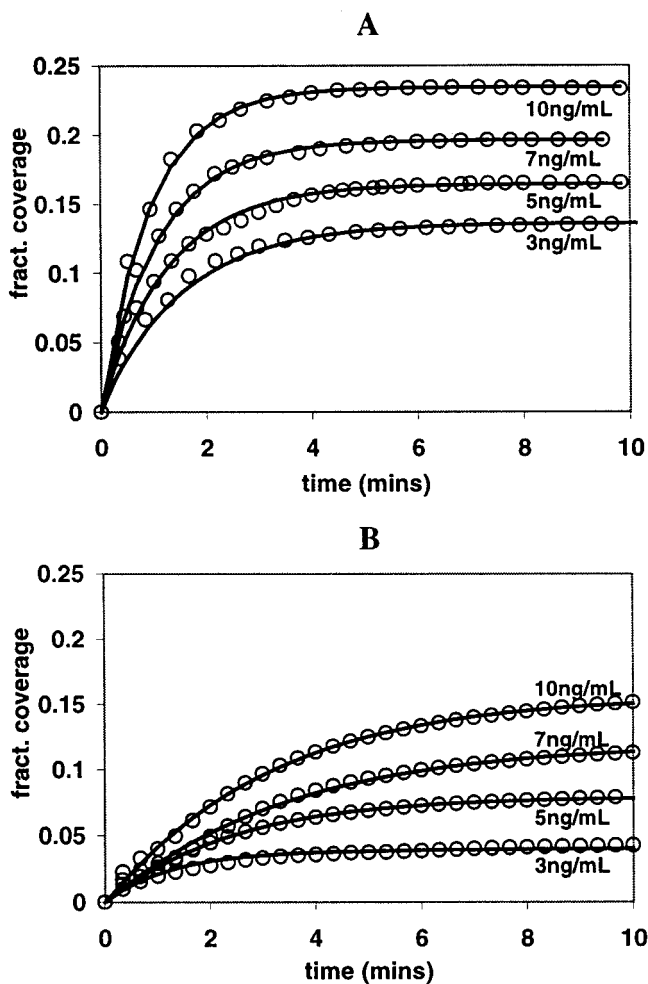


Figure 4. Comparison of the two-compartment model (solid lines) with experimental data recorded under flowing conditions in the absence (A) and presence (B) of glycerol. The experimental data (circles) are the same data presented in Figure 3B.

and the expected values for these parameters suggests that the two-compartment model also provides a good quantitative description of the kinetic data. The differences in the k_m values between the experiments with and without glycerol agree with what one would expect on the basis of the difference in the viscosity between the PBS and the PBS/glycerol mixtures. In addition, estimates of the binding site density agree with the results from separate radiolabeling measurements of antibody density ($\sim 10^{-9}$ – 10^{-8} mol/m²). The larger values of $c_{b,sat}$ obtained in the presence of glycerol are due to fiber-to-fiber variations in antibody loading.

Our transport-kinetic model was applied to the experiments done in the absence of flow. The data for these experiments and the least-squares fits to our model appear in Figure 5. Estimates for the model's adjustable parameters are listed in Table 3. The transport-kinetic model provides a good qualitative and quantitative description of the kinetic data. Estimates of the forward and reverse rate constants are comparable to the values produced by the two-compartment approach. Besides k_f and k_r , our model also provides estimates for the analyte diffusivity and the binding site density. The values that we obtained for these parameters are again reasonable. Values for the binding site density agree with separate radiolabeling measurements of the antibody density. Also, the values for analyte diffusivity are comparable to estimates based

on the size of the analyte and the viscosities of the PBS and PBS/glycerol buffers. ($D \sim 10^{-9}$ m²/s for PBS and $\sim 10^{-10}$ m²/s for PBS/glycerol).¹³ Moreover, the change in D between the PBS and PBS/glycerol mixtures is consistent with the change in viscosity between these two solutions.

DISCUSSION

In all of our experiments, mass transport limitations were more important when glycerol was present in the analyte solutions. In addition to the dependence of the binding dynamics on the flow rate (Table 1), the estimated values of rate constants that appear in Tables 1–3 support this conclusion. For the experiments done with glycerol, the well-mixed model yielded on and off rates that were smaller than those predicted by our transport-kinetic model. However, the same estimated values for the experiments done in PBS are comparable. The rate constants in the well-mixed model are accurate only when the kinetics are reaction-rate-limited. When analyte binding is transport-limited, the well-mixed model yields k_f and k_r values that erroneously reflect the rate of diffusion and convection to the fiber surface. As a result, the kinetic parameters in this model can be functions of the flow rate and the analyte's diffusivity. The two-compartment model, however, includes a description of analyte transport as well as the reaction kinetics. Variations in the flow rate or transport properties of the analyte can be accounted for by adjusting k_m . Similarly, our transport-kinetic model describes the diffusion of analyte to the fiber surface. If extended, the model could also describe how the flow rate can affect the binding dynamics. Because the later two models describe analyte transport, they provide estimates of the kinetic parameters that reflect the true, intrinsic reaction kinetics and are independent of the flow rate and the analyte's diffusivity. For our experiments in glycerol, the binding dynamics are diffusion-limited, and the transport rate is thus slower than the rate of binding. The rate constants estimated with the transport-kinetic and two-compartment models therefore exceed those from the well-mixed model. In the experiments with PBS, there are no apparent diffusion limitations, and the rate constants in all three models describe the intrinsic reaction kinetics. All three models thus yield comparable estimates for the kinetic parameters.

The two-compartment model is easier to apply than our transport-kinetic model. To use the two-compartment approach, one only needs to solve a single ordinary differential equation. Solving this equation requires less computational effort than solving the diffusion equation that governs our transport-kinetic model. Since both models yield similar estimates for the analyte's kinetic and transport properties, our model does not necessarily yield more accurate parameter estimates. There would therefore appear to be no advantage to using our more computationally intense model. Nevertheless, our transport-kinetic model is still an improvement over the two-compartment approach. It can be applied to experiments done without flow. Also, if extended, it can also be used to analyze kinetics with flow. The two-compartment model, however, can only be applied when analyte flows over the sensor surface. The ability to analyze experiments without flow may be especially useful when an experimentalist only has a small amount of analyte available to characterize a

(13) Bird, R. B.; Stewart, W. E.; Lightfoot, E. N. *Transport Phenomena*; John Wiley and Sons: 1960.

Table 2. Parameters Estimated with the Two-Compartment Model for the Experiments Done without Flow^a

concn. ng/mL	PBS				PBS + glycerol			
	k_f , $10^5 \text{ M}^{-1}/\text{s}^{-1}$	k_r , 10^{-2} s^{-1}	$c_{b,\text{sat}}$, $10^{-9} \text{ mol}/\text{m}^2$	k_m , $10^{-6} \text{ m}^2/\text{s}$	k_f , $10^5 \text{ M}^{-1}/\text{s}^{-1}$	k_r , 10^{-2} s^{-1}	$c_{b,\text{sat}}$, $10^{-9} \text{ mol}/\text{m}^2$	k_m , $10^{-6} \text{ m}^2/\text{s}$
3	6.8 ± 0.5	1.3 ± 0.06	1.5 ± 0.4	5.6 ± 0.2	4.1 ± 0.3	2.8 ± 0.1	9.6 ± 0.5	1.5 ± 0.1
5	5.2 ± 0.1	1.3 ± 0.03	1.7 ± 0.09	4.7 ± 0.3	4.2 ± 0.1	2.4 ± 0.05	11 ± 0.3	1.6 ± 0.05
7	5.0 ± 0.09	1.5 ± 0.03	1.0 ± 0.03	5.5 ± 0.2	4.5 ± 0.1	2.3 ± 0.08	15 ± 0.7	1.5 ± 0.06
10	5.0 ± 0.08	1.7 ± 0.03	1.8 ± 0.06	4.8 ± 0.3	3.7 ± 0.09	2.0 ± 0.05	13 ± 0.3	1.3 ± 0.04

^a Error estimates are calculated from each parameter's standard error.

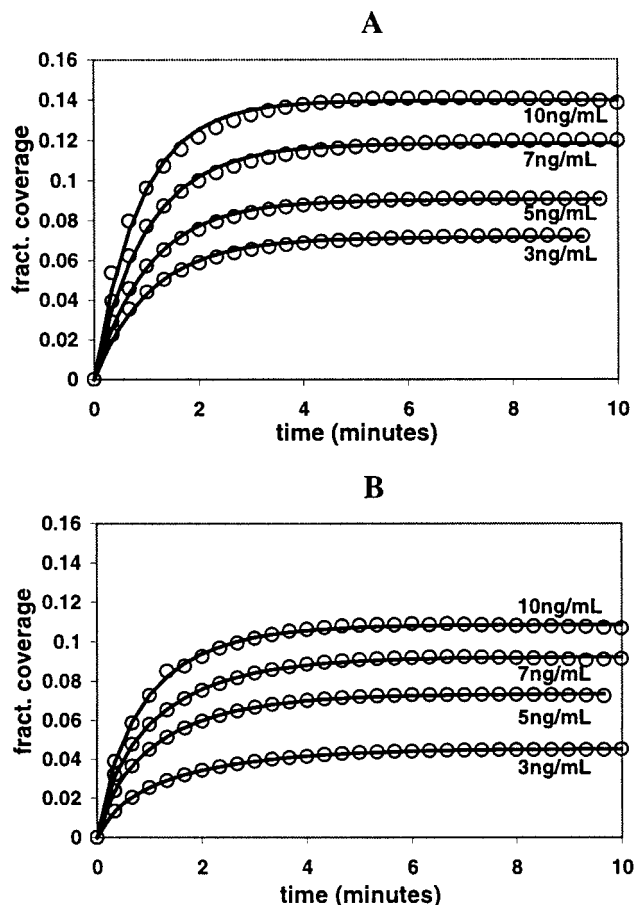


Figure 5. Kinetic data from experiments done in the absence of flow in PBS (A) and in solutions containing PBS with 60 wt % glycerol (B). Experimental data are indicated by the open circles while least-squares fits to our transport-kinetic model are denoted by the solid lines.

biomolecular interaction. Under these circumstances, one cannot afford to continuously flow analyte through the sensor. More importantly, the two-compartment model characterizes the analyte's transport properties with a phenomenological transport rate constant, k_m . This parameter is somewhat ambiguous as its value depends on the geometry of the sensor as well as the analyte's transport properties. One typically relies on experimental correlations or simplified theoretical analyses to estimate k_m .³ In contrast, our transport-kinetic model does not rely on a phenomenological description of mass transport. In our model, analyte transport is controlled by the analyte's diffusivity D . Since this parameter is directly measurable and independent of the sensor configuration, it is easier to provide an initial guess for this parameter in the

least-squares fitting routine. In addition, since D is measurable, it is also easier to judge the accuracy of the final, fitted parameters with our model than with the two-compartment approach.

The error estimates for the parameters in Tables 2 and 3 are artificially small. These estimates are calculated from each parameter's standard error. Therefore, these error estimates only reflect the scatter or noise within each experiment. Fiber-to-fiber variations exceed the scatter within the data. Hence, the actual error in each parameter is most likely larger than the values that we report here.

The accuracy of the rate constants, diffusivities, and antibody densities that one would estimate with our model depends on the sensitivity of the kinetic data to each of these parameters. If binding does not exhibit transport limitations, then the data will be sensitive to the kinetic rate constants and to the binding site density but completely insensitive to the analyte's diffusivity. Conversely, if binding is highly transport-limited, the data will only be a function of the analyte's diffusivity. Previous studies have attempted to achieve sensitivity to both the kinetic and transport properties by simultaneously fitting data from several experiments done with different binding site densities.^{2,3} By varying $c_{b,\text{sat}}$, one can control the relative importance of mass transport limitations.^{4,14} If a suitable range of binding site densities is chosen, one can obtain a set of data that is a function of both the transport and kinetic properties. A global analysis of these data will therefore be sensitive to all of the model parameters.

We did not perform this type of analysis. Instead, the data from each experiment were analyzed separately. Despite this, the values listed in Tables 2 and 3 suggest that the data are sensitive to all of the model parameters. The Damköler number $\kappa = k_f c_{b,\text{sat}} h / D$ (transport-kinetic model) or $\kappa = k_f c_{b,\text{sat}} / k_m$ (two-compartment model), a nondimensional parameter, which indicates the relative rates of reaction and diffusion, is ~ 1 for the experiments with glycerol. This indicates that the reaction kinetics and analyte diffusion are equally important. Thus, the data should be sensitive to the model parameters that describe analyte transport (D) as well as the parameters that describe the reaction kinetics (k_f , k_r , $c_{b,\text{sat}}$). In PBS, κ is ~ 10 , and the kinetic data are more sensitive to the rate constants and binding site density than the analyte's diffusivity. In this case, we expect that the estimates for the kinetic parameters are more accurate than those for the analyte's transport properties.

In addition to fitting data corresponding to different binding site densities at the same time, previous global analyses have also simultaneously fit kinetic data from multiple assays done with

(14) Schuck, P.; Minton, A. P. *Anal. Biochem.* **1996**, *240*, 262–272.

Table 3. Parameters Estimated with the Transport–Kinetic Model for the Experiments Done without Flow^a

concn, ng/mL	PBS				PBS + glycerol			
	k_f , $10^5 \text{ M}^{-1} \text{ s}^{-1}$	k_r , 10^{-2} s^{-1}	$C_{b,\text{sat}}$, 10^{-9} mol/m^2	D , $10^{-10} \text{ m}^2/\text{s}$	k_f , $10^5 \text{ M}^{-1} \text{ s}^{-1}$	k_r , 10^{-2} s^{-1}	$C_{b,\text{sat}}$, 10^{-9} mol/m^2	D , $10^{-10} \text{ m}^2/\text{s}$
3	4.1 ± 0.5	1.4 ± 0.06	5.1 ± 0.4	20 ± 0.2	4.2 ± 0.3	2.3 ± 0.08	9.6 ± 0.3	3.3 ± 0.1
5	3.2 ± 0.3	1.5 ± 0.06	4.3 ± 0.3	19 ± 0.2	4.2 ± 0.09	2.3 ± 0.04	8.5 ± 0.1	4.2 ± 0.04
7	3.4 ± 0.2	1.6 ± 0.08	5.1 ± 0.3	9.4 ± 0.05	4.5 ± 0.07	2.6 ± 0.05	11 ± 0.1	4.1 ± 0.04
10	2.9 ± 1.0	1.7 ± 0.1	4.3 ± 1.0	17 ± 0.5	3.2 ± 0.1	2.4 ± 0.08	8.2 ± 0.2	4.2 ± 0.1

^a Error estimates are calculated from each parameter's standard error.

different analyte concentrations. We attempted to do this with the data in Figures 3–5, but were unable to obtain satisfactory fits. One reason that this approach may have failed is that the rate constants may vary with analyte concentration due to heterogeneity in the association kinetics. Since the antibody is randomly oriented on the fiber surface in our experiments, the binding kinetics are most likely described by a distribution of rate constants. At low analyte concentrations, the most accessible binding sites dominate the binding. As the analyte concentration is increased, the less accessible sites become important and the apparent rate constants decrease. To obtain reliable parameters from such global fits, it will be necessary to eliminate these effects. Modifying the immobilization chemistry to control the antibody orientation on the fiber surface can do this.

Current efforts are aimed at expanding the versatility of our transport-kinetic model. So far, we have only applied our model to the analysis of association kinetics in the absence of flow. We intend to extend our model to analyze association kinetics under flow as well as unbinding data. In addition, while we have shown that our model can be used to analyze data, we will extend it so that it can be used as a predictive tool. For example, one could use the model's data analysis capabilities to estimate the model parameters from experimental data. By solving the governing equations in the model, it is then possible to (1) predict a priori how perturbations in these parameters will impact the biosensor's response and (2) optimize future biosensor experiments.

In summary, we have shown that is feasible to analyze biosensor data with our proposed model. Application of the model yielded reasonable estimates for the reaction rate constants, Cy5-TNB diffusivity, and binding site density in the presence and absence of observable mass-transfer limitations. Unlike the simpler well-mixed and two-compartment models, the spatial distribution of analyte does not restrict the applicability of the model presented in this work. Thus, our model involves fewer assumptions, is more versatile, and can allow one to access experimental conditions that would be intractable with previously existing transport-kinetic models.

ACKNOWLEDGMENT

The work described in this paper was supported by the Office of Naval Research (N10014-96-1-339). We thank Ms. Lisa Shriver-Lake and Ms. Saskia Van Bergen for their assistance with the Analyte 2000 immunosensor. In addition, we thank Prof. Johannes M. Nitsche for his help with the mathematical modeling of the biosensor experiment.

Received for review June 18, 1999. Accepted September 27, 1999.

AC990672B